Precision Agric
DOI 10.1007/s11119-016-9486-1

Effect of observation scale on remote sensing based estimates of evapotranspiration in a semi-arid row cropped orchard environment

Nandita Gaur[1] · Binayak P. Mohanty[1] · Shawn C. Kefauver[2]

Abstract Understanding in detail the spatial distribution of evapotranspiration (ET) in row cropped fruit production areas with diverse water requirements is vital for monitoring water use and efficient irrigation scheduling. Spatially distributed ET for these environments can be estimated using remote sensing (RS). However, the computation of RS based ET under such conditions is complicated because of the complex parameterizations that are required to derive ET for the mixed pixels comprising of bare soil and well-watered plants typical of row cropped areas. Also, the parameterization of these processes is not scale invariant, owing to change in the percentage of vegetation cover in the mixed pixels across remote sensing observation scales. In this study, our main objectives were (1) to isolate and evaluate the effect of varying spatial scales (comparable to canopy sizes and larger) of the remote sensing data on ET estimates; and (2) provide an operational method for estimating remote sensing based ET for row cropped conditions. ET was computed using an empirical technique (S-SEBI: Simplified-Surface Energy Balance Index Algorithm) for almond and pistachio orchards from remote sensing imagery collected at a scale comparable to the canopy sizes of the trees (5.8 and 7.2 m) and a scale that was much larger than the canopy size (120 m) using the MASTER and Landsat sensors, respectively. In order to account for the effect of mixed pixels, a Normalized Difference Vegetation Index based correction factor was applied to the derived ET values and the results averaged for different fields were validated with Penman–Monteith based ET estimates. It was found that the corrected mean ET estimates at 120 m were in agreement with the Penman–Monteith based ET estimates ($RMSE_{average} = 0.12$ mm/h), whereas they were underestimated at the finer resolutions. Our results indicated that a remote sensing pixel resolution comparable to the row spacing and smaller and comparable to the canopy size overestimated the land surface

✉ Nandita Gaur
nandita.gaur@tamu.edu

[1] Department of Biological and Agricultural Engineering, Texas A&M University, 2117 TAMU, 301C Scoates Hall, College Station, TX 77843, USA

[2] Integrative Crop Ecophysiology Group, University of Barcelona, Av. Diagonal, 643, 08028 Barcelona, Spain

Published online: 08 December 2016

temperature and consequently, underestimated ET when using operational models that do not account for vegetation and soil temperature separately. The results of the application of the NDVI correction factor indicates that good spatial estimates of crop ET can be made for crops growing in orchards using simple ET models that require minimal data and freely available Landsat imagery. These findings are very encouraging for the regular monitoring of crop health and effective management of irrigation water in highly water stressed agricultural environments.

Keywords S-SEBI · Scale · Evapotranspiration · Remote sensing · Orchards

Introduction

Agriculture in water stressed and semi-arid environments is sustained through irrigation. In order to effectively manage water resources in such areas, the use of irrigation water needs to be optimized by minimizing water losses. Evapotranspiration (ET) accounts for up to 80% of the water losses in semi-arid regions (Chehbouni et al. 2008) and thus, an accurate estimation of ET can lead to better determination of the water losses by plants to enable effective management of irrigation planning.

The most extensively and successfully applied method for estimating crop ET (ET_c) for irrigation systems planning is the two-step crop coefficient (K_c) x reference ET (ET_{ref}) method (Allen and Pereira 2009; Pruitt and Doorenbos 1977; Allen et al. 1998). This method provides numerically accurate ET estimates in basin wide studies without any spatial representation of ET. Also, the estimation of K_c becomes complicated when the percent crop cover, irrigation techniques and routines vary across the region (Allen and Pereira 2009). In irrigated fruit production areas where the fertilizer treatments, irrigation techniques and age of various trees within the area (and consequently water demands) are often variable, a numerically accurate spatial representation of ET is highly desirable. This can be achieved through properly validated ET estimates from remote sensing, which provides spatial representation of ET while preserving the numerical accuracy of the crop coefficient based methodology (Price 1990; Kustas et al. 1994; Bastiaanssen et al. 1998; Roerink et al. 2000; McCabe and Wood 2006).

Remote sensing data is available at multiple spatial scales, which determine the amount of detail that can be extracted from each dataset. In an agricultural set-up of corn and soybean, McCabe and Wood (2006) found that ET estimates from LANDSAT-ETM (60 m) and ASTER (90 m) were consistent and had good correlation, while MODIS (1020 m) was not a good platform for field scale ET owing to its inability to discriminate land-surface heterogeneity. Kustas et al. (2004) demonstrated that remote sensing derived ET estimates at scales varying from 60 m to 960 m were comparable with the in situ measurements, but that the coarser resolution sensors made it impossible to distinguish field scale fluxes from different crops. Other studies have also indicated that under full crop cover conditions, there is loss in spatial information as the scale coarsens (Mauser and Schadlich 1998); however, row cropped environments like fruit orchards consist of evenly spaced trees where a large amount of bare soil is exposed between the trees. Higher discrepancies in ET estimates based on remote sensing data at different scales have been observed under such conditions owing to the more complex parameterization of the energy balance processes (Chang and Hong 2012; Moran et al. 1997). In this study, it was hypothesized that in row cropped environments, finer resolution imagery does not imply more accurate ET estimates from the dataset when using operational single source ET models. The land surface temperature estimates from smaller mixed pixels (pixel resolution comparable to canopy size and row spacing) can be higher on average than that obtained from a coarser mixed pixel where the pixel resolution is much larger than the canopy size. This could occur since a pixel resolution comparable to the canopy size and row spacing would lead to the presence of a higher fraction of bare soil in most pixels (example- pistachio canopy in Fig. 1a) and thus lead to higher land surface temperature estimates (and consequently, underestimate ET) as opposed to a coarser pixel (Fig. 1b). Thus, the size of the pixel or observation scale would affect the ET value estimated from a remote sensing dataset. Since land-surface temperature is a major input in ET estimating algorithms, this variability due to scale will impact most algorithms used to derive remote sensing based ET unless the soil and canopy temperatures are accurately accounted for separately.

In this study, the Simplified- Surface Energy Balance Index (S-SEBI) algorithm (Roerink et al. 2000) was used to estimate ET. As an empirical approach, S-SEBI is inherently region-specific, but also consequently removes compounding errors that may be incurred due to incorrect parameterization of energy balance processes in complex settings, such as partial vegetation cover. S-SEBI requires minimal data inputs and assumptions in order to estimate ET; however, in the absence of inputs required by more complex process based algorithms, and given the incomplete understanding of the scaling of those processes in remote sensing, such an empirical algorithm may prove to be more accurate and also more suitable to addressing the hypotheses of this study. Furthermore, S-SEBI is compatible with multiple sensors and works well for various land covers. It was successfully employed by Sobrino et al. (2007) and Verstraeten et al. (2005) over diverse landscapes using AVHRR imagery, and Roerink et al. (2000) developed this algorithm using Landsat imagery. More recently, S-SEBI was deemed useful in a semi-arid irrigated environment in Mexico (Chirouze et al. 2014).

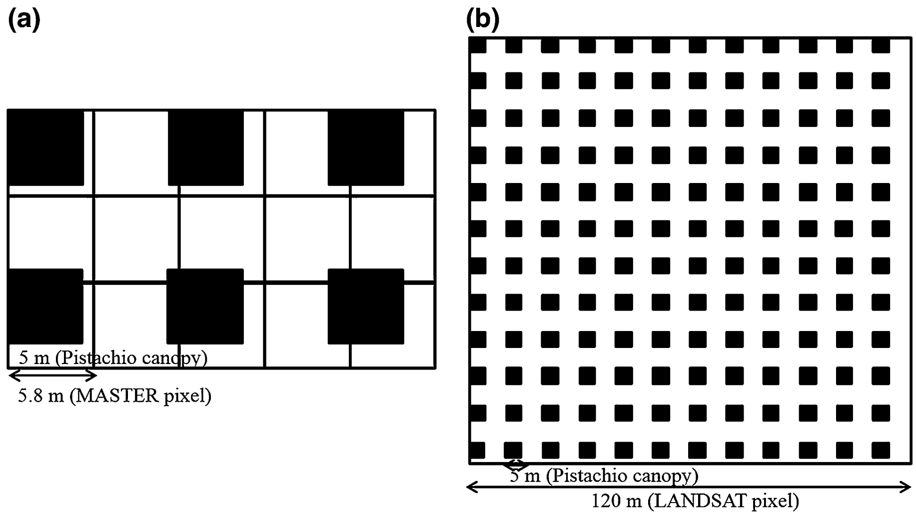

Fig. 1 Conceptual diagram representing relative size of average mature pistachio canopies and remote sensing pixels

The objective of the study was to assess the scaling behavior of ET by comparing spatially distributed ET derived from high resolution (comparable to canopy size) and relatively coarser (containing multiple tree canopies per pixel) remote sensing imagery with MODIS based (1 km) and Penman-Montieth (fetch scale) based ET estimates in row cropped conditions. A correction factor that explicitly reduces the discrepancy between measured, ground based ET and ET derived from remote sensing imagery under row cropped conditions was also developed to improve ET estimates under semi-arid, row cropped conditions.

Materials and methods

Study area

The study was conducted in almond and pistachio orchards in Lost Hills, Kern County, California (Fig. 2). The climate of the region is semi-arid, with summer months that are extremely hot and dry with virtually no precipitation and with most crop water demands fulfilled by irrigation. The study area comprised of four adjacent orchards planted in rows and irrigated through fanjet and drip irrigation. The pistachio orchards were planted in the year 2000 with a row spacing of 5.8 m. The two almond orchards were planted one year apart (1999 and 2000) with a row spacing of 7.5 m. The almond trees varied from 2.5 to 7.0 m high, whereas the pistachio trees were shorter, with heights varying between 1.5 and 3.0 m. (Cheng et al. 2013).

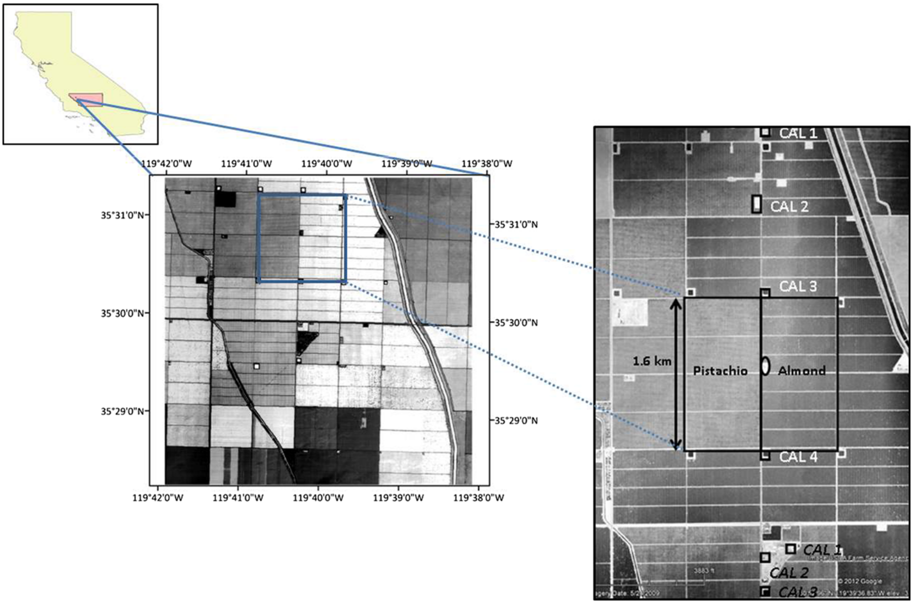

Fig. 2 Location and imagery of the study orchards in California. The calibration sites marked in *white* represent calibration sites for 2009 while those marked in *black* represent calibration sites for 2010. The *encircled area* is a bare dry patch in the almond field

Remote sensing platforms

The study uses imagery from two different remote sensing platforms – an airborne sensor, MASTER (MODIS/ASTER airborne simulator), and a space borne sensor, Landsat 5. The MASTER imagery was collected on July 24th, 2009 (7.2 m resolution, time of overpass ~2 P.M. local time) and June 29th, 2010 (5.8 m resolution, time of overpass ~10:30 A.M. local time) as part of the Student Airborne Research Program (SARP) campaign organized by NASA in collaboration with the National Sub-Orbital Education and Research Center, whereas the Landsat (120 m thermal band resolution, time of overpass ~10:30 A.M. local time) imagery was collected on July 28th, 2009 and June 29th, 2010. The LANDSAT imagery was provided by the U.S. Geological Survey (USGS) and was processed using the software version LPGS_12.1.1. The necessary calibration data for the remote sensing imagery was collected at the field site as part of the SARP campaign.

Landsat

Landsat 5 terrain corrected imagery (path 42, row 35) was corrected to surface reflectance using the Fast Line-of-Sight Atmospheric Analysis of Spectral Hypercubes (FLAASH) module for basic atmospheric correction provided by ENVI version 4.3 (Exelis Visual Information Solutions, Boulder, Colorado). The atmospheric model chosen for the correction was set to 'Tropical' based on the climate of the Central Valley. The aerosol model was selected as 'Rural' and the initial visibility was set to 40 km since our datasets comprised of clear, haze free days in an agricultural non-urban area. The procedure used to extract at-satellite temperature values from Landsat was adopted from Landsat 7- Science Data User's Handbook, NASA (Irish 2000). The procedure for deriving actual land surface temperature from at-satellite temperature by accounting for surface emissivity of the respective pixels is detailed below.

Per-pixel emissivity was determined based on the red (R) and near infrared (NIR) bands using the technique developed by Valor and Caselles (1996). The various assumed emissivity components used in the calculation were obtained from those developed for fruit trees.

$$\varepsilon_0 = \varepsilon_v P_v + \varepsilon_g (1 - P_v) + 4(d\varepsilon) P_v (1 - P_v) \tag{1}$$

$$P_v = \frac{1 - NDVI/NDVI_g}{\left(1 - NDVI/NDVI_g\right) - k\left(1 - NDVI/NDVI_v\right)} \tag{2}$$

$$k = \frac{\rho_{2v} - \rho_{1v}}{\rho_{2g} - \rho_{1g}} \tag{3}$$

ε: dimensionless emissivity of the pixel, $d\varepsilon$: cavity effect of a rough surface (Caselles and Sobrino 1989) ~0.04, P_v: Vegetation fraction cover, ρ_2: reflectance in NIR band, ρ_1: reflectance in R band, $NDVI = \left(\frac{NIR-R}{NIR+R}\right)$, normalized difference vegetation index (Tucker 1979).

The sub-scripts '0', 'g' and 'v' refer to the pixel under consideration, a bare ground pixel and a fully vegetated pixel, respectively. The values of emissivity for a bare ground pixel and fully vegetated pixel were assumed to be 0.95 and 0.99. These values are in agreement with values reported in literature.

The uncalibrated land surface temperature was obtained by correcting the at-satellite (radiative) surface temperature for emissivity effects of the surface

$$T_0 = \sqrt[4]{T_{sat}^4 / \varepsilon_0} \tag{4}$$

T_0 = Uncalibrated land surface temperature, T_{sat} = At-satellite temperature

The remote sensing based land surface temperature was calibrated using with the temperature data collected on the ground using empirical line correction (ELC). Ground truth data (as described in "Field data collection" section) was collected on July 22nd 2009 and June 29th, 2010. The equations developed to calibrate the derived temperature estimates to the actual land surface temperature are given below in Eqs. 5 and 6 ($R^2 > 0.9$).

$$T_{act} = 3.7156 \cdot T_0 - 96.093\ (2009) \tag{5}$$

$$T_{act} = 2.2632 \cdot T_0 - 46.918\ (2010) \tag{6}$$

T_0 = Uncalibrated derived land surface temperature, °C, T_{act} = Calibrated derived land surface temperature, °C

MODIS/ASTER airborne simulator (MASTER)

The MASTER sensor collects information over 50 optical and thermal wavelengths. The temperature estimates for the MASTER sensor were derived from band 42 which corresponded to the peak of the thermal signature. Atmospheric correction using MODTRAN 4 and the In-Scene Atmospheric Compensation (ISAC) algorithm for 2009 and 2010 respectively, were applied to the thermal imagery prior to ELC and temperature estimation. A constant emissivity value of 0.975 was used in the temperature derivation for the MASTER sensor. A standard MODTRAN 4 and FLAASH correction for optical bands was applied for 2009 and 2010, respectively. The equations used to calibrate the derived temperatures from MASTER to land surface temperature in 2009 and 2010 are given below in Eqs. 7 and 8 respectively.

$$T_{act} = 1.3184 \cdot T_0 - 20.229\ (2009) \tag{7}$$

$$T_{act} = 0.7194 \cdot T_0 + 10.204\ (2010) \tag{8}$$

T_0 = Uncalibrated derived land surface temperature, °C, T_{act} = Calibrated derived land surface temperature, °C

Field data collection

Ground truth land surface temperature was collected using the Fluke 572 thermal infrared (TIR) guns (Fluke Electronics, Washington, USA) to calibrate the remote sensing derived temperature. The emissivity for the calibration of the TIR gun was set to 0.95 based on its radiometer range (8–14 μm). A blackbody calibration was also done to account for any variability in emissivity of the targets. In 2009, 4 target locations (2 bare soil and 2 water bodies) in the field were chosen to calibrate the imagery (Fig. 2). Each target location was divided in a 3 by 3 grid and the temperature of all 9 grid points was estimated using the TIR gun. This was done twice through the afternoon. The mean temperatures of the grid points are provided in Fig. 3. Since each location was sampled twice, a linear relationship between temperature and time of temperature collection was assumed (Fig. 3a). The

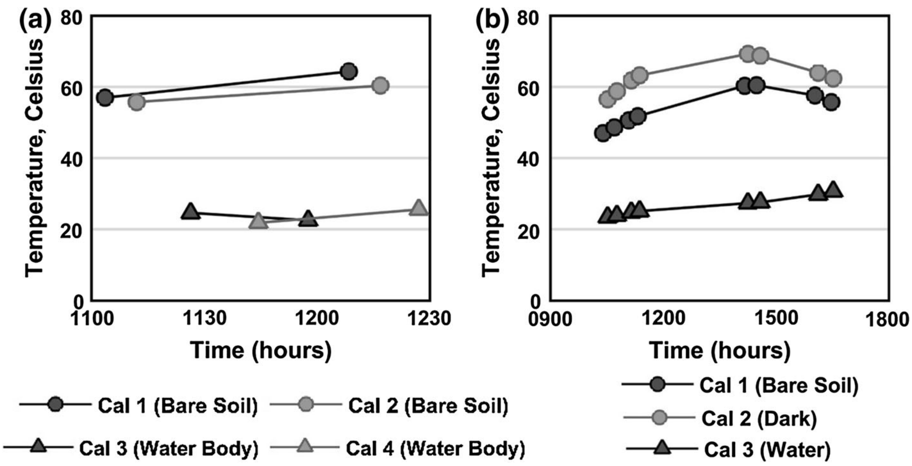

Fig. 3 Calibration curves for estimation of ground temperature at the time of satellite and airborne sensor overpass in **a** 2009 and **b** 2010

temperature of the ground at the time of over pass of the sensor was estimated from this curve. Three such targets (light, dark and water), each divided into a 2 by 2 grid were chosen to calibrate the imagery in 2010 (Fig. 2). This was done 8 times through the afternoon. The temperature of each location at the time of overpass was estimated using the fitted polynomial curve as shown in Fig. 3b.

The value of hourly incoming solar radiation (Table 1) and reference ET estimates were obtained from weather station No. 146 (Belridge) managed by California Irrigation Management Information System (CIMIS). The station is located 800 m west of the pistachio orchards. CIMIS generates ET estimates for the state of California and calculates reference ET over a standard grass or alfalfa land cover using the modified Penman equation (Pruitt and Doorenbos 1977). The necessary crop coefficients required to compute ET estimates specific to the crop were also calculated by CIMIS based on the technique developed by Allen et al. (1998).

Estimating ET

Energy balance method: S-SEBI

A brief description of S-SEBI, with minor variations in computation of albedo, is provided below for completeness. However, readers are referred to (Roerink et al. 2000) for details of the algorithm.

Table 1 Incoming solar radiation (CIMIS, Belridge station)

Date	Solar Rad (W m^{-2})
July 24th, 2009	835.1
July 28th, 2009	834.2
June 29th, 2010	858.9

$$R_n = G + H + LE \tag{9}$$

R_n = Net radiation, W/m^2, H = Sensible heat flux, W/m^2, LE = Latent heat flux, W/m^2, G = Soil heat flux, W/m^2

Incoming solar radiation, R_S was measured close to the field site at weather station No. 146 managed by CIMIS. R_n was estimated using the relationship given below

$$R_n = R_S(1 - \alpha) + R_{ld} - R_{lu} \tag{10}$$

α = Dimensionless albedo, R_{ld} = Long-wave downwards radiation (W m^{-2}) (Brutsaert 1975)

$$R_{ld} = \varepsilon_a \sigma T_a^4 \left(\mathrm{W\ m^{-2}}\right) \tag{11}$$

T_a = Air temperature (K), ε_a = Dimensionless atmospheric emissivity

$$\varepsilon_a = 1.24\left(\frac{e_a}{T_a}\right)^{1/7} \tag{12}$$

ε_a = Vapor Pressure (mBar), R_{lu} = Long-wave upwards radiation defined as

$$R_{ld} = \varepsilon_S \sigma T_S^4 \left(\mathrm{W\ m^{-2}}\right) \tag{13}$$

ε_s = Land Surface emissivity (calculated in Eq. 1), σ = Stefan–Boltzman Constant (W m^{-2} K^{-4}), T_s = Land surface temperature (°K)

Soil heat flux, G, was estimated as a function of NDVI using the model developed by Daughtry et al. (1990) and assuming that the same relationship held good for our field site. The use of a vegetation based relationship for calculating soil heat flux was justifiable since the area under consideration was an agricultural region.

$$G = (0.325 - 0.208NDVI)R_n \tag{14}$$

The evaporative fraction (Λ) was assumed constant through the day (Shuttleworth et al. 1989; Brutsaert and Chen 1996; Crago 1996) for the S-SEBI model and was calculated as:

$$\Lambda = \left(\frac{T_H - T_0}{T_H - T_{\lambda E}}\right) \tag{15}$$

where,

$$T_H = a_H + b_H r_0 \; T_{\lambda E} = a_{\lambda E} + b_{\lambda E} r_0 \tag{16}$$

Λ: Evaporative fraction corresponding to pixel albedo r_0, T_H: Theoretical land surface temperature for an albedo value when all available energy is converted to sensible heat, $T_{\lambda E}$: Theoretical temperature for a land-surface albedo value when all available energy is converted to latent heat, a_H, b_H, $a_{\lambda E}$, $b_{\lambda E}$: fitting parameters (Roerink et al. 2000).

These fitting parameters were obtained by bounding the albedo versus temperature graphs as shown for the MASTER and Landsat sensors (Fig. 4). The accuracy of the bounding lines is subject to the nature of the heterogeneity present in the area (i.e. presence of light and dark pixels). Ideally, the light pixels should correspond to bare soil that is completely devoid of moisture whereas the dark pixels should correspond to pure water pixels. These pixels were chosen from the water and bare ground targets that were also used for calibration (Fig. 2). Albedo, r_0, was estimated using the model listed in Gowda et al. (2008) that utilizes the Red (R) and Near Infrared bands (NIR).

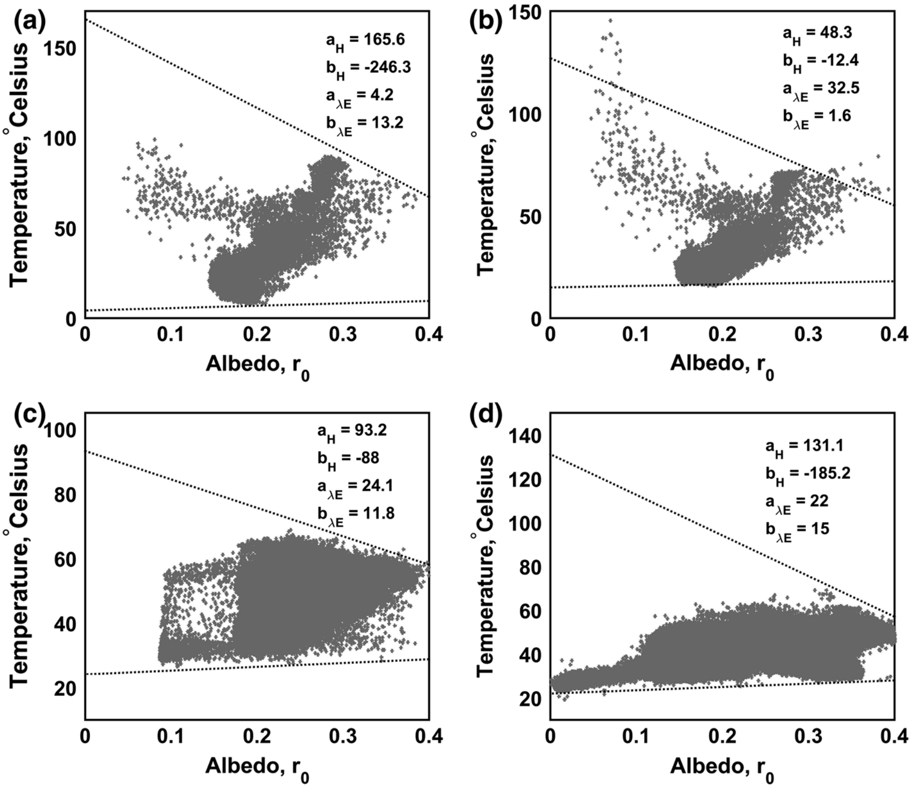

Fig. 4 Albedo v/s land surface temperature for **a** Landsat sensor, 2009, **b** Landsat sensor, 2010, **c** MASTER sensor, 2009, and **d** MASTER sensor, 2010

$$r_0 = 0.512R + 0.418NIR \tag{17}$$

where, NIR = Band 4 (Landsat) or Band 9 (MASTER), R = Band 3 (Landsat) or Band 5 (MASTER).

The *latent heat, (LE)* was estimated as

$$LE = \Lambda(R_n - G) \tag{18}$$

The latent heat flux was converted to ET estimates (mm/h) using Eqs. 19 and 20 (Henderson-Sellers 1984).

$$ET_{S-SEBI} = LE\left(\frac{3600}{L}\right) \tag{19}$$

where,

$$L = 2.5e^6 - 2.386e^3(T - 273.15)\ (\text{Henderson - Sellers 1984}) \tag{20}$$

T = Land surface temperature (°K).

Correction factor for S-SEBI based ET

In order to correct for the partial vegetation cover, the ET values estimated using S-SEBI were adjusted based on the percent vegetation cover (Eq. 21).

$$ET = \frac{ET_{S-SEBI}}{\left(\frac{NDVI}{NDVI_{\max}}\right)} \tag{21}$$

$\frac{NDVI}{NDVI_{\max}}$ = percent vegetation cover, $NDVI$ = NDVI of the pixel under consideration, $NDVI_{max}$ = NDVI of a completely vegetated pixel or maximum NDVI of the region (with similar leaf area index as the crop under consideration), $ET_{S\text{-}SEBI}$ = modelled ET estimates (mm/h).

Results and discussion

Effect of correction factor on ET estimates

ET obtained from S-SEBI is based on the relationship between land surface temperature and albedo data derived at pixel resolution of the remote sensor and as such gives an estimate of the water loss per pixel (which may be fully or partially vegetated). This relationship, however, holds good only for homogeneous pixels whose albedo changes proportionally to the temperature (also water content) of the entire pixel. In the given study, the bare soil around the canopy and within the rows was parched dry and as a result each pixel was comprised of the well-watered trees and soil at different temperatures. Under such conditions, the resultant albedo/temperature of the mixed (partially vegetated) pixel would not change in proportion with the water content of the pixel. A well-watered plant in such conditions may appear to be water stressed because of the higher temperature of the mixed pixel due to the presence of hot and dry bare soil in it. Thus, the ET values in the pixel will be underestimated as a result of averaging of temperatures of the different components in the mixed pixel. The correction factor applied to ET estimates was based on the assumption that the ET increases in proportion to the NDVI of the pixel and was designed to increase the estimated ET value to match a fully vegetated pixel. The Penman–Monteith based ET estimates also provide an accurate estimate of the potential water loss from a crop with complete ground cover (unless a variation of percent ground cover is accounted for in the computation of Kc). Thus, such a correction also enables the comparison and validation of the estimated ET with the more accurate Penman–Monteith based ET values while retaining the spatial variability and detail in ET estimates from remote sensing platforms.

Figure 5a and b show the ET derived using S-SEBI from the Landsat and MASTER sensor in 2010. On average, ET losses from the almond fields were higher as compared to the pistachio fields. However, the derived ET values were underestimated due to the bare soil fraction in each pixel. By scaling the ET as given in Eq. 21, water losses from the plants were calculated (Fig. 5c, d), which were higher than the averaged (uncorrected) ET across the mixed pixel. The increase in corrected ET values was larger for the pistachio orchards as compared to almond orchards (Fig. 5) since pistachios had a smaller canopy and consequently consisted of more bare soil compared to almond pixels.

The field averages and standard deviation for ET (Fig. 6a, b) and corrected ET (Fig. 6c, d) for the years 2009 and 2010 are plotted against Penman–Monteith based ET_c (K_c x

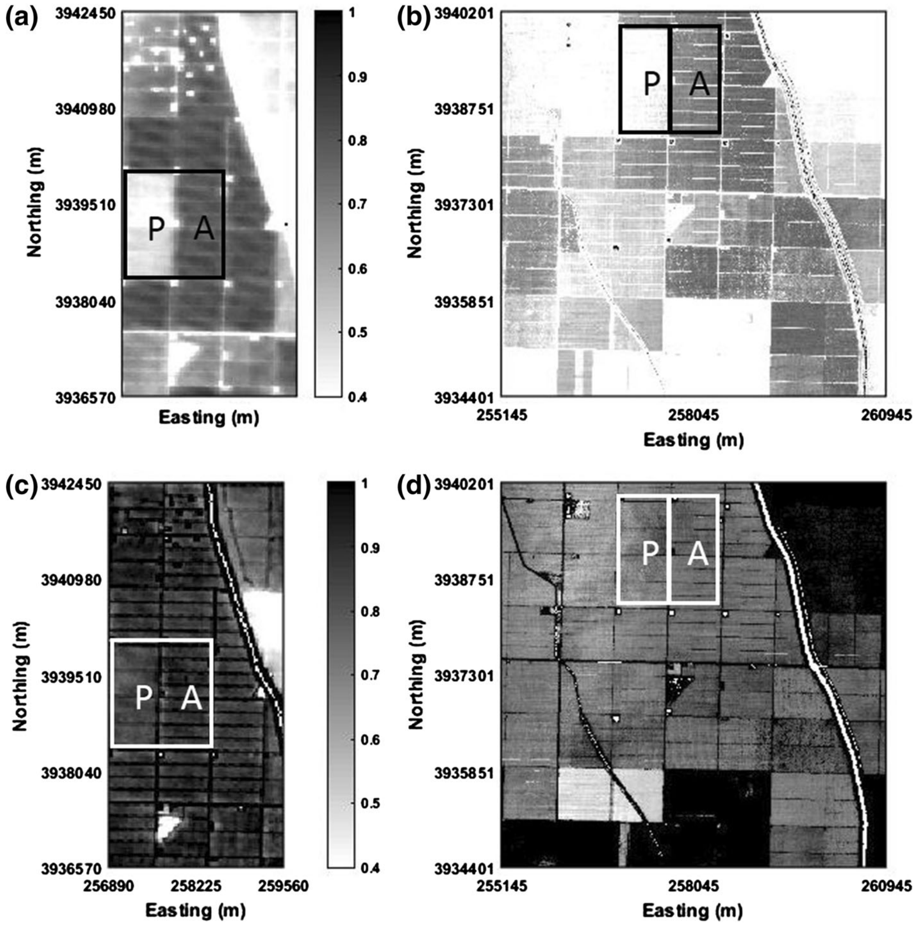

Fig. 5 ET (S-SEBI estimated) distribuition in 2010 as estimated from **a** Landsat and **b** MASTER sensor and Corrected ET distribution in 2010 **c** Landsat and **d** MASTER sensor. (P-pistachio and A-almonds)

ET_{ref}) estimates (Table 2). The calculation of ET based on a reference crop (ET_{ref}, either from clipped, well-watered grass or a taller full-cover alfalfa crop) has been standardized by Food and Agriculture Organization (FAO), (Allen et al. 1998; 2006) and the American Society of Civil Engineers (ASCE-EWRI 2005). K_c is the crop specific coefficient representing ratio of the crop's potential ET (ET_c) and ET_{ref}. This formulation does not account for agricultural practices like planting in rows that result in partial ground cover. The orchards in our study area were not under water stress and the trees were expected to be transpiring nearly at the potential (Penman–Monteith) rate; however, S-SEBI generated ET estimates were lower than the Penman–Monteith based estimates (Fig. 6a, b). Low ET estimates were also reported for the 2009 imagery by Roy et al. (2013) who used the SEBAL model to derive ET. ET from pistachio orchards that comprise of trees with smaller canopies was underestimated more than that from the almond trees with larger canopies in both the years. After applying the correction for percent crop cover, the ET estimates became comparable with the Penman–Monteith based estimates (Fig. 6c, d). The observed root mean square error (RMSE) for pistachios changed from 0.65 to 0.08 and

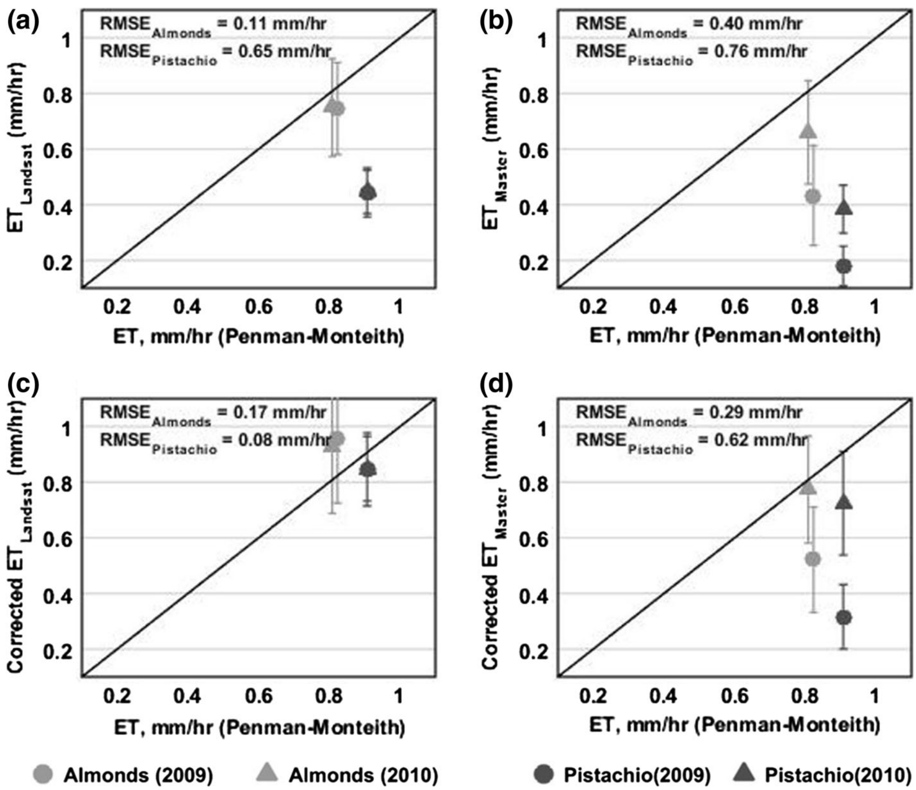

Fig. 6 Average ET values in 2009 and 2010 before correcting for partial vegetation cover for **a** Landsat and **b** MASTER and after correcting for partial vegetation cover for **c** Landsat and **d** MASTER

Table 2 CIMIS (Belridge station) based ET estimates

Date	Crop	ET_0 (mm/h)**	Crop Coefficient, Kc*	ET = Kc x ET_0 (mm/h)
July 24th, 2009	Almonds	0.762	1.08	0.823
July 28th, 2009	Almonds	0.762	1.08	0.823
June 29th, 2010	Almonds	0.762	1.06	0.808
July 24th, 2009	Pistachio	0.762	1.19	0.907
July 28th, 2009	Pistachio	0.762	1.19	0.907
June 29th, 2010	Pistachio	0.762	1.19	0.907

* Crop coefficients were chosen based on time of year and have been provided by CIMIS for mature almond crops

** Provided by CIMIS

0.76 to 0.62 mm/h for Landsat and MASTER, respectively. The difference in RMSE for almonds was lower. Thus, we assume that better accounting for percent vegetation cover improves estimates of remote sensing derived ET in orchard conditions using S-SEBI. This finding is very encouraging for remote sensing based ET estimation over agricultural orchards in California that solely depend on irrigation, since spatial estimates of ET can be obtained with the use of simple models like S-SEBI and routinely available Landsat (and eventually the most recent Sentinel-2) data. The resulting precision in ET estimates may also then be used to design targeted irrigation schemes.

Effect of varying scale on ET estimates

ET estimates using remote sensing data are largely affected by plant structure, leaf area index, canopy characteristics and proportion of bare soil present in a pixel. Variation in these factors with varying resolution of the pixels affects different portions of the electromagnetic spectrum differently. Stagakis et al. (2012) evaluated the effect of varying pixel resolution (from sunlit crown level to aggregated with bare soil) for various physiological indices based on the optical electromagnetic spectrum. They found that the relationship of the indices with plant water stress deteriorated by the inclusion of bare soil in the aggregated pixels. In order to compare the Landsat and MASTER based ET, the distribution of corrected ET as obtained from both sensors in 2009 (Fig. 7a) and 2010 (Fig. 7b) was plotted through violin plots. The ET of crops from the MASTER sensor was normally distributed while Landsat based ET was slightly right skewed. The normality of the ET values indicates that most trees were transpiring at the same rate. The thin-tailed right skew (higher values) in the LANDSAT based ET may be attributed to the inevitable averaging of bare soil/road around the fields. The corrected ET values for such pixels are higher since the NDVI is lower. Numerically, ET estimates obtained from MASTER were lower than those obtained from Landsat. The higher contrast between the two sensors in 2009 could be because of differences in irrigation amounts on the two days when imagery was collected. Table 3 provides the mean and variance for the distribution of the MASTER-based S-SEBI calculated ET values. The MASTER sensor provided lower mean ET estimates than Landsat during both the years. However, in 2010, when the imagery from MASTER and Landsat was collected almost simultaneously, the differences between the two ET estimates were smaller. The variance values for the pistachio fields in 2009 were almost the same at both resolutions, implying that the variance captured at 7.2 and 120 m resolution was nearly similar in the orchards. On the other hand, the differences

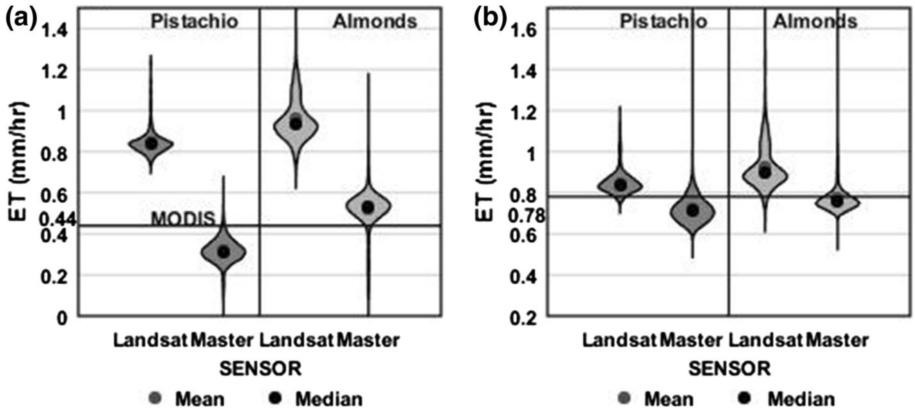

Fig. 7 Violin plots representing distrbution of ET in the year **a** 2009 and **b** 2010. *Red line* depicts MODIS based average ET (Color figure online)

Table 3 Mean (Variance) of corrected ET estimates obtained for almonds and pistachio from Landsat and MASTER

Crop	Landsat	MASTER
Year: 2009		
Almonds	0.96 (0.013)	0.52 (0.009)
Pistachio	0.84 (0.004)	0.32 (0.003)
Year: 2010		
Almonds	0.93 (0.014)	0.77 (0.009)
Pistachio	0.85 (0.003)	0.72 (0.009)

between the variances at the two scales was higher in 2010. More data at different scales would be required to accurately ascertain the cause of the difference in variance, but it could be attributed to difference between the sensor resolution and canopy sizes. The sensor resolution in 2009 was 7.2 m (larger than a typical mature pistachio canopy) whereas it was approximately same (5.8 m) as a mature pistachio canopy in 2010. The difference in resolution could alter the percent vegetation cover per pixel, which creates differences in variance. The difference in variance for the larger almond canopy at the two scales was consistent across the two years (higher for 120 m).

The underestimation of mean ET by MASTER can also be attributed to the pixel resolution of the sensors (Landsat, 120 m thermal; MASTER, 5.8 m). McCabe et al. (2008) showed that for a 50:50 split binary mixed pixel with large temperature variation between the two components, the retrieved temperature (between 8 and 12 µm) could vary up to 2 degrees K. They found this variation to be an increasing function of the difference in mean and standard deviation of the temperature of the binary components. The pixels in our study area represent binary mixtures with a large difference in mean temperature of the well irrigated trees and dry bare soil. The Landsat pixel was large enough to comprise of multiple trees and the ET estimates that resulted were an average of trees and bare soil (Fig. 1b). On the other hand, the small pixel resolution of the MASTER sensor at most allowed one tree per pixel (Fig. 1a). Most pixels for the MASTER sensor consisted of either (1) a portion of a tree and bare soil or, in some cases, (2) only bare soil. This led to higher pixel temperatures in the MASTER sensor and consequently S-SEBI generated lower ET estimates from MASTER. The results indicate that, similar to the typical loss of information in upscaling, there may be loss of information in selecting resolutions that are comparable to canopy sizes under row orchard conditions. The MODIS based ET values (Fig. 7) were typically lower than Landsat and higher than the MASTER sensor derived ET. The MODIS pixel has a resolution of 1 km and, under the given agricultural settings, comprises various crops that differ in terms of growth stage, irrigation patterns and types. Thus, at the scale of a MODIS pixel, the representativeness of an agricultural field is lost.

The above analysis indicates that in the specific case of row cropped conditions, the spatial resolution of remote sensing data can lead to under/over estimation of ET. It is also not necessarily true that finer resolution of remote sensing data will enable better estimation of ET using single source ET algorithms.

Conclusions

In the given study, we evaluated the effect of varying spatial resolutions on ET estimates for two different crop orchards in California. Actual ET was estimated over almond and pistachio orchards using S-SEBI algorithm. We employed MASTER sensor data at a resolution of 5.8 and 7.2 m and from the Landsat sensor data at 120 m resolution at similar dates from two consecutive years. We found that Landsat provided more accurate estimates of ET than MASTER, which tended to underestimate the ET from the plants. An NDVI based correction technique was also applied to correct for the mixed pixel effects in the orchard conditions, which improved ET estimates with respect to the crop coefficient method. A comparison of the derived ET estimates with MODIS based ET estimates revealed that MODIS based ET estimates do not compare well with the ET estimates from individual crop types because of its coarse pixel size. The results from this study are limited to two days of data in the growing season with specific view angles. The issue of scale in remote sensing, especially for partially vegetated fields, complicates as the viewing and sun angles are altered. Therefore, additional analysis needs to be conducted before applying these results for other seasons and using different remote sensing platforms with non-nadir view angles. The results of the study are however very encouraging toward the incorporation of remote sensing data in estimating evapotranspiration in the region for use toward precision agriculture. This research may be of particular interest as it shows how freely available Landsat data can be used in conjunction with a simple ET model with minimal data requirements to provide ET and related crop health maps to farmers regularly.

Acknowledgement The effort of Nick Clinton in atmospherically correcting the MASTER data and Cassie Knierim in providing calibrated MASTER land surface temperatures (2009) is acknowledged as is the effort of the entire agricultural group from the Student Airborne Program held in 2009 and 2010 and Blake Sanden, for collecting ground truth data. The data for the MASTER sensor was obtained as part of the Student Airborne Research Program, organized by NSERC in collaboration with NASA. The authors would also like to thank the organizers and mentors of the SARP program – Rick Shetter and Dr. Susan L. Ustin. Finally, we acknowledge the funding support of NASA Earth and Space Science Fellowship (NNX13 AN64H), NASA THPs (NNX08AF55G and NNX09AK73G) and NSF (DMS-09-34837) grants.

References

Allen, R. G., & Pereira, L. S. (2009). Estimating crop coefficients from fraction of ground cover and height. *Irrigation Science, 28*(1), 17–34. doi:10.1007/s00271-009-0182-z.

Allen, R. G., Pereira, L. S., Raes, D., & Smith, M. (1998). Crop evapotranspiration-guidelines for computing crop water requirements-FAO Irrigation and drainage paper 56. FAO, Rome 300: 6541. http://www.fao.org/docrep/X0490E/X0490E00.htm. Accessed 5 Dec 2016.

Allen, R. G., Pruitt, W. O., Wright, J. L., Howell, T. A., Ventura, F., Snyder, R., et al. (2006). A recommendation on standardized surface resistance for hourly calculation of reference ETo by the FAO56 Penman-Monteith method. *Agricultural Water Management, 81*(1), 1–22. doi:10.1016/j.agwat.2005.03.007.

Bastiaanssen, W., Menenti, M., Feddes, R. A., & Holtslag, A. A. M. (1998). A remote sensing surface energy balance algorithm for land (SEBAL). 1. Formulation. *Journal of Hydrology, 212,* 198–212. doi:10.1016/S0022-1694(98)00253-4.

Brutsaert, W. (1975). On a derivable formula for long-wave radiation from clear skies. *Water Resources Research, 11*(5), 742–744. doi:10.1029/WR011i005p00742.

Brutsaert, W., & Chen, D. (1996). Diurnal variation of surface fluxes during thorough drying (or severe drought) of natural prairie. *Water Resources Research, 32*(7), 2013–2019. doi:10.1029/96WR00995.

Caselles, V., & Sobrino, J. È. A. (1989). Determination of frosts in orange groves from NOAA-9 AVHRR data. *Remote Sensing of Environment, 29*(2), 135–146. doi:10.1016/0034-4257(89)90022-9.

Chang, N. B., & Hong, Y. (2012). *Multiscale hydrologic remote sensing: Perspectives and applications*. Boca Raton: CRC Press Inc.

Chehbouni, A., Escadafal, R., Duchemin, B., Boulet, G., Simonneaux, V., Dedieu, G., et al. (2008). An integrated modelling and remote sensing approach for hydrological study in arid and semi-arid regions: The SUDMED Programme. *International Journal of Remote Sensing, 29*(17–18), 5161–5181. doi:10.1080/01431160802036417.

Cheng, T., Riaño, D., Koltunov, A., Whiting, M. L., Ustin, S. L., & Rodriguez, J. (2013). Detection of diurnal variation in orchard canopy water content using MODIS/ASTER airborne simulator (MASTER) data. *Remote Sensing of Environment, 132,* 1–12. doi:10.1016/j.rse.2012.12.024.

Chirouze, J., Boulet, G., Jarlan, L., Fieuzal, R., Rodriguez, J. C., Ezzahar, J., et al. (2014). Intercomparison of four remote-sensing-based energy balance methods to retrieve surface evapotranspiration and water stress of irrigated fields in semi-arid climate. *Hydrology and Earth System Sciences, 18,* 1165–1188. doi:10.5194/hess-18-1165-2014.

Crago, R. (1996). Conservation and variability of the evaporative fraction during the daytime. *Journal of Hydrology, 180*(1–4), 173–194. doi:10.1016/0022-1694(95)02903-6.

Daughtry, C. S. T., Kustas, W. P., Moran, M. S., Pinter, P. J., Jr., Jackson, R. D., Brown, P. W., et al. (1990). Spectral estimates of net radiation and soil heat flux. *Remote Sensing of Environment, 32*(2–3), 111–124. doi:10.1016/0034-4257(90)90012-B.

Gowda, P. H., Chavez, J. L., Colaizzi, P. D., Evett, S. R., Howell, T. A., & Tolk, J. A. (2008). ET mapping for agricultural water management: Present status and challenges. *Irrigation Science, 26*(3), 223–237. doi:10.1007/s00271-007-0088-6.

Henderson-Sellers, B. (1984). A new formula for latent heat of vaporization of water as a function of temperature. *Quarterly Journal of the Royal Meteorological Society, 110*(466), 1186–1190. doi:10.1002/qj.49711046626.

Irish, R. R. Landsat 7 science data users handbook. National Aeronautics and Space Administration, Report (2000): 430-15

Kustas, W., Li, F., Jackson, T. J., Prueger, J. H., MacPherson, J. I., & Wolde, M. (2004). Effects of remote sensing pixel resolution on modeled energy flux variability of croplands in Iowa. *Remote Sensing of Environment, 92*(4), 535–547. doi:10.1016/j.rse.2004.02.020.

Kustas, W., Perry, E., Doraiswamy, P. C., & Moran, M. S. (1994). Using satellite remote sensing to extrapolate ET estimates in time and space over a semiarid rangeland basin. *Remote Sensing of Environment, 49*(3), 275–286. doi:10.1016/0034-4257(94)90022-1.

Mauser, W., & Schadlich, S. (1998). Modelling the spatial distribution of ET on different scales using remote sensing data. *Journal of Hydrology, 212,* 250–267. doi:10.1016/S0022-1694(98)00228-5.

McCabe, M. F., Balick, L. K., Theiler, J., Gillespie, A. R., & Mushkin, A. (2008). Linear mixing in thermal infrared temperature retrieval. *International Journal of Remote Sensing, 29*(17–18), 5047–5061. doi:10.1080/01431160802036474.

McCabe, M. F., & Wood, E. F. (2006). Scale influences on the remote estimation of ET using multiple satellite sensors. *Remote Sensing of Environment, 105*(4), 271–285. doi:10.1016/j.rse.2006.07.006.

Moran, M. S., Humes, K. S., & Pinter, P. J., Jr. (1997). The scaling characteristics of remotely-sensed variables for sparsely-vegetated heterogeneous landscapes. *Journal of Hydrology, 190*(3), 337–362. doi:10.1016/S0022-1694(96)03133-2.

Price, J. C. (1990). Using spatial context in satellite data to infer regional scale evapotranspiratoin. *IEEE Transactions on Geoscience and Remote Sensing, 28*(5), 940–948. doi:10.1109/36.58983.

Pruitt, W.O. & Doorenbos, J. (1977). *Proceeding of the International Round Table Conference on "Evapotranspiration"*. Budapest, Hungary.

Roerink, G., Su, Z., & Mementi, M. (2000). S-SEBI: A simple remote sensing algorithm to estimate the surface energy balance. *Physics and Chemistry of the Earth, Part B: Hydrology, Oceans and Atmosphere, 25*(2), 147–157. doi:10.1016/S1464-1909(99)00128-8.

Roy, S., Ophori, D. & Kefauver, S. (2013). Estimation of actual evapotranspiration using surface energy balance algorithms for land model: A case study in San Joaquin Valley, California. *Journal of Environmental Hydrology*, *21*, Paper 14.

Shuttleworth, W. J., Gurney, R. J., Hsu, A. Y., & Ormsby, J. P. (1989). FIFE: The variation in energy partition at surface flux sites. *IAHS Publication, 186,* 67–74.

Sobrino, J. A., Gómez, M., Jiménez-Muñoz, J. C., & Olioso, A. (2007). Application of a simple algorithm to estimate daily evapotranspiration from NOAA–AVHRR images for the Iberian Peninsula. *Remote Sensing of Environment, 110*(2), 139–148. doi:10.1016/j.rse.2007.02.017.

Stagakis, S., González-Dugo, V., Cid, P., Guillén-Climent, M. L., & Zarco-Tejada, P. J. (2012). Monitoring water stress and fruit quality in an orange orchard under regulated deficit irrigation using narrow-band structural and physiological remote sensing indices. *ISPRS Journal of Photogrammetry and Remote Sensing, 71,* 47–61. doi:10.1016/j.isprsjprs.2012.05.003.

Tucker, C. J. (1979). Red and photographic infrared linear combinations for monitoring vegetation. *Remote Sensing of Environment, 8*(2), 127–150. doi:10.1016/0034-4257(79)90013-0.

Valor, E., & Caselles, V. (1996). Mapping land surface emissivity from NDVI: Application to European, African, and South American areas. *Remote Sensing of Environment, 57*(3), 167–184. doi:10.1016/0034-4257(96)00039-9.

Verstraeten, W., Veroustraete, F., & Feyen, J. (2005). Estimating evapotranspiration of European forests from NOAA-imagery at satellite overpass time: Towards an operational processing chain for integrated optical and thermal sensor data products. *Remote Sensing of Environment, 96*(2), 256–276. doi:10.1016/j.rse.2005.03.004.